Development 138, 3431-3440 (2011) doi:10.1242/dev.065029

A late phase of germ plasm accumulation during *Drosophila* oogenesis requires Lost and Rumpelstiltskin

Kristina S. Sinsimer, Roshan A. Jain*, Seema Chatterjee and Elizabeth R. Gavis†

SUMMARY

Asymmetric mRNA localization is an effective mechanism for establishing cellular and developmental polarity. Posterior localization of *oskar* in the *Drosophila* oocyte targets the synthesis of Oskar to the posterior, where Oskar initiates the assembly of the germ plasm. In addition to harboring germline determinants, the germ plasm is required for localization and translation of the abdominal determinant *nanos*. Consequently, failure of *oskar* localization during oogenesis results in embryos lacking germ cells and abdominal segments. *oskar* accumulates at the oocyte posterior during mid-oogenesis through a well-studied process involving kinesin-mediated transport. Through live imaging of *oskar* mRNA, we have uncovered a second, mechanistically distinct phase of *oskar* localization that occurs during late oogenesis and results in amplification of the germ plasm. Analysis of two newly identified *oskar* localization factors, Rumpelstiltskin and Lost, that are required specifically for this late phase of *oskar* localization shows that germ plasm amplification ensures robust abdomen and germ cell formation during embryogenesis. In addition, our results indicate the importance of mechanisms for adapting mRNAs to utilize multiple localization pathways as necessitated by the dramatic changes in ovarian physiology that occur during oogenesis.

KEY WORDS: Nanos, Oskar, Germ plasm, mRNA localization, Rumpelstiltskin, Lost, *Drosophila*

INTRODUCTION

Intracellular mRNA localization is a conserved mechanism for generating protein asymmetries that are necessary for developmental polarity and polarized cell functions. In a variety of organisms, maternally synthesized mRNAs that are localized within the oocyte and embryo produce regionalized distributions of proteins required for patterning of the embryonic axes, specification of germ layers and formation of the germ line (Gavis et al., 2007). Localization of maternal *oskar* (*osk*) mRNA to the posterior of the *Drosophila* oocyte restricts the synthesis of Osk protein to the posterior, where Osk initiates the assembly of the germ plasm (Ephrussi et al., 1991; Markussen et al., 1995; Rongo et al., 1995). This specialized cytoplasm, which contains germ cell fate determinants, persists at the posterior into early embryogenesis, where it induces formation of the pole cells, the germ cell progenitors. The germ plasm is also essential for development of the anterior-posterior body axis, through its role in posterior localization and translational activation of the abdominal determinant *nanos* (*nos*) (Ephrussi et al., 1991; Gavis and Lehmann, 1992; Gavis and Lehmann, 1994).

As a maternal mRNA, *osk* is transcribed in the ovarian nurse cells and is transported from the nurse cells into the oocyte early in oogenesis (stages 1-7 of 14 morphologically defined stages) (Ephrussi et al., 1991; Kim-Ha et al., 1991). During mid-oogenesis (stages 8-10), reorganization of the oocyte microtubule cytoskeleton creates a posterior bias of microtubule plus-ends that allows net posteriorly directed transport of *osk* by kinesin motors (Theurkauf et al., 1992; Brendza et al., 2000; Zimyanin et al., 2008). After reaching the posterior pole, *osk* is translated into two functionally distinct Osk isoforms: one recruits additional germ plasm proteins, including the highly conserved RNA helicase Vasa (Vas), whereas the other maintains the localization of *osk* mRNA and Osk protein through an actin-dependent mechanism (Markussen et al., 1995; Rongo et al., 1995; Breitwieser et al., 1996; Vanzo and Ephrussi, 2002; Vanzo et al., 2007).

A second posterior localization pathway, acting later in oogenesis when the nurse cells initiate apoptosis and extrude or 'dump' their contents into the oocyte (stages 11 and 12), mediates localization of *nos* (Forrest and Gavis, 2003). Microtubule-based transport to the posterior is preempted by the reorganization of microtubules into cortical bundles that mediate the concerted streaming of the oocyte cytoplasm to mix nurse cell and oocyte contents (Theurkauf et al., 1992). Instead, *nos* moves with the bulk cytoplasm during ooplasmic streaming and becomes trapped by association with germ plasm components at the posterior (Forrest and Gavis, 2003). The integration of *nos* into the germ plasm activates *nos* translation and creates a protein gradient that directs abdominal development during embryogenesis (Gavis and Lehmann, 1992). In mutants for germ plasm components such as *osk* or *vas*, *nos* mRNA fails to localize to the posterior, Nos protein is not produced and, consequently, embryos lack abdominal segments (Gavis and Lehmann, 1994; Wang et al., 1994).

The ability of an mRNA to utilize a particular localization pathway is thought to depend on its cadre of associated localization factors. These include proteins that recognize cis-acting localization signals usually found within 3′ untranslated regions (3′UTRs), accessory proteins that package these RNA-protein (RNP) complexes into higher order particles, and adaptors that link the RNP particles to the cytoskeleton for transport and/or anchoring (Gavis et al., 2007; Lewis and Mowry, 2007; Kugler and Lasko, 2009). Genetic and biochemical approaches have identified numerous proteins that interact directly or indirectly with *osk* mRNA and are required for assembly, transport, and/or anchoring of *osk* RNP particles. Several of these factors are also involved in the localization of two other mRNAs, *bicoid* (*bcd*) and *gurken*

Department of Molecular Biology, Princeton University, Princeton, NJ 08544, USA.

*Present address: Department of Cell and Developmental Biology, University of Pennsylvania School of Medicine, Philadelphia, PA 19104, USA
†Author for correspondence (gavis@princeton.edu)

Accepted 31 May 2011

(*grk*), whose respective dynein-dependent transport to the anterior and dorso-anterior regions of the oocyte occurs concomitantly with *osk* transport (Kugler and Lasko, 2009). These studies and studies of localized mRNAs in other cell types support a model in which localized RNAs are recognized and packaged by a combination of general and RNA-specific factors, with the particular combination of factors dictating how and where the RNP particles are transported and anchored.

We previously identified the *Drosophila* heterogeneous ribonucleoprotein M (hnRNPM) homolog Rumpelstiltskin (Rump) as a direct-acting *nos* localization factor (Jain and Gavis, 2008). Here, we report the characterization of a second protein, Lost, which co-purifies with *nos* and Rump and contributes to *nos* localization. Surprisingly, our analysis of *rump* and *lost* double mutants has uncovered a second phase of *osk* localization that occurs concomitant with *nos* localization during late oogenesis and has not been previously described. This late-acting pathway, but not *osk* localization during mid-oogenesis, requires the combined functions of Rump and Lost. Moreover, our results reveal that localization of *osk* during mid-oogenesis is not sufficient for *osk*-dependent germ plasm function in either anterior-posterior body axis or pole cell formation. Rather, the Rump- and Lost-dependent posterior accumulation of *osk* during late oogenesis results in an amplification of the germ plasm that ensures wild-type abdominal and germline development. We show that Rump binds directly to *osk* as well as to *nos*, suggesting that Rump and Lost are part of a core localization complex that promotes utilization of the late localization pathway by multiple mRNAs in parallel.

MATERIALS AND METHODS

Fly stocks

The following mutants and transgenic lines were used: *y* w^{67c23} (Lindsley and Zimm, 1992), osk^{A87} (Vanzo and Ephrussi, 2002), $CG14648^{ZCL3169}$ (Morin et al., 2001), *gfp-vas* (Johnstone and Lasko, 2004), *osk-(ms2)*$_6$ (Lin et al., 2008), *hsp83-MCP-GFP* (Forrest and Gavis, 2003), *hsp83-MCP-RFP* (Weil et al., 2006) and *nos-(ms2)*$_{18}$ (Brechbiel and Gavis, 2008).

Genetic analysis of *lost*

CG14648 is referred to as *growl* in FlyBase. The $lost^1$ allele was generated by imprecise P element excision of the GFP protein-trap insertion $CG14648^{ZCL3169}$. Individual males, each bearing an excision in trans to *Df(3R)ME15*, which deletes the *lost* locus, were screened by PCR using primer pairs to amplify regions immediately upstream or downstream of the P element. Deletion endpoints were then mapped by PCR amplification and sequencing. The $lost^1$ $rump^1$ double mutant was generated by meiotic recombination. The *lost* rescue transgene consists of a 5.7 kb *Xba*I-*Xho*I genomic fragment isolated from BAC clone BACR30G03 (Berkeley *Drosophila* Genome Project) and inserted into pCaSpeR4 (Pirotta, 1988).

Production of MBP-Lost and anti-Lost monoclonal antibodies

The *lost* coding region (minus the initiation codon) was PCR amplified from cDNA LD30155 (Rubin et al., 2000) with the addition of 5′ *Bam*HI and 3′ *Hin*dIII sites and cloned into the pMal-c2 vector (New England Biolabs) using the same sites to generate an in-frame fusion of Lost to the C-terminus of maltose-binding protein (MBP). MBP-Lost was expressed in *Escherichia coli* and purified on amylose/agarose resin (New England Biolabs). Anti-Lost monoclonal antibodies were generated as described previously (Kalifa et al., 2006) using uncleaved MBP-Lost as the antigen.

Immunoprecipitations and immunoblot analysis

Ovary extract was prepared as described previously (Kalifa et al., 2009), using IP buffer [25 mM HEPES (pH 7.4), 150 mM NaCl, 2.5 mM $MgCl_2$, 0.5 mM EDTA, 0.01% Triton X-100, 1 × complex protease inhibitor cocktail (Roche) and 10 μg/ml pepstatin] supplemented with phosphatase inhibitors (1 mg/ml sodium vanadate, 20 mM sodium fluoride). Extracts were pre-cleared using Dynabeads Protein G (Invitrogen) for 1 hour at 4°C and then incubated for 2 hours at room temperature with Dynabeads Protein G-bound with Rump 5G4 monoclonal antibody (Jain and Gavis, 2008) or anti-Lost 1D11 monoclonal antibody. Beads were washed six times with IP buffer. Purified protein complexes were fractionated by SDS-PAGE, transferred to nitrocellulose membrane, and detected by immunoblotting and chemiluminescence. Final primary antibody concentrations were: 1:30,000 for rabbit anti-Khc (Cytoskeleton), 1:10,000 for mouse anti-Snf (gift of P. Schedl, Princeton University, NJ, USA), 1:3000 for rabbit anti-Osk (Vanzo and Ephrussi, 2002); 1:4000 for mouse anti-Rump and 1:1000 for mouse anti-Lost. Mouse TrueBlot Ultra (eBiosciences) secondary antibody was used at 1:1000 to limit detection of heavy chain. Quantification was performed using ImageJ (NIH).

For RNA co-immunoprecipitations, beads were resuspended in IP buffer and treated with RQ1 DNase (Promega), then RNA was extracted by Tri-Reagent (Sigma):chloroform, and ethanol precipitated. RNA was reverse transcribed using SuperScript II reverse transcriptase (RT) (Invitrogen) and oligo (dT) primer per the manufacturer's instructions. 'No RT' control samples were treated similarly except that reverse transcriptase was omitted. Primers used for RT-PCR of *osk* are shown in Table S1 in the supplementary material.

UV-crosslinking assays

The *osk* 5′UTR, 3′UTR and subdivisions of the 3′UTR were amplified from *osk* cDNA with the addition of a 5′ T7 primer sequence using primers shown in Table S1 in the supplementary material. The *nos* +2′ element probe has been previously described (Jain and Gavis, 2008). Synthesis of radiolabeled RNA probes and UV-crosslinking was performed as described previously (Bergsten et al., 2001).

In situ hybridization and immunofluorescence

In situ hybridization for *nos*, *osk* and *bcd* in 0- to 2-hour-old embryos was performed as described previously (Gavis and Lehmann, 1992). Fluorescence in situ hybridization (FISH) for *osk* in oocytes was performed as described in Vanzo and Ephrussi (Vanzo and Ephrussi, 2002) except that ovaries were fixed in 4% electron microscopy (EM) grade formaldehyde in PBS, subsequent washes and antibody incubations were performed in PBST (PBS + 0.1% Tween-20) and hybridization steps were performed at 55°C. Anti-digoxigenin-rhodamine (1:200, Roche) and DAPI (1:1000, Molecular Probes) were used to visualize the *osk* probe and nuclei, respectively.

Anti-Vas immunofluorescence was performed on 3- to 5-hour-old embryos as described (Becalska et al., 2011) using rabbit anti-Vasa (1:10,000; gift from P. Lasko, McGill University, Montreal, Canada), goat anti-rabbit-Alexa 488 (1:1000) and DAPI (1:1000, Molecular Probes). Pole cells were counted from images taken at 1.5 μm intervals throughout the embryo posterior with a Zeiss LSM 510 confocal microscope, 40×/1.3 NA objective. Microtubules were detected as described previously (Becalska and Gavis, 2010). For visualization of F-actin, ovaries were fixed in 4% EM grade formaldehyde in PBS, washed 3×5 minutes in PBS, blocked in PBT (PBS/1% Tween-20/2% BSA) for 30 minutes, stained with Alexa Fluor 488 phalloidin (1:500 in PBT) for 30 minutes and washed 3×10 minutes in PBS. Microtubules and actin were imaged with a Leica SP5 confocal microscope, using a 63×/1.4 NA oil immersion objective.

Live imaging

Live imaging of germ plasm components was performed as described in Weil et al. (Weil et al., 2006). Images were collected with a Leica SP5 confocal microscope using a 63×/1.4 NA oil immersion objective. Ooplasmic streaming was visualized as described in Becalska et al. (Becalska and Gavis, 2010).

Fluorescence quantification

All fluorescence intensity measurements in live oocytes were made using Volocity 5.3 (Improvision). For quantification of *osk*GFP* and GFP-Vas accumulation at the posterior in live oocytes, confocal *z*-stacks of 1.5 μm optical sections spanning 25-30 μm at the posterior cortex were taken every 15-20 minutes starting prior to nurse cell dumping (stage 10B) and continuing for 3 hours, after the cessation of nurse cell dumping (late stage 12/early stage 13). For each oocyte, a threshold based on the auto-

fluorescence detected in the oocyte cytoplasm was set and only fluorescence above this threshold was quantified. The total fluorescence at the oocyte posterior at each time point was then normalized to time zero and the net change in fluorescence accumulation was calculated $[(t_3–t_0)/t_0]$.

The total volume occupied by *osk*GFP* at the posterior was quantified from *z*-stacks of 1.5 μm sections taken through the entire posterior of the oocyte at either stage 10A or stage late12/early 13. All wild-type and *lost⁻ rump⁻* oocytes of the same stage were imaged in the same imaging session under identical conditions. For each stage, a single fluorescence intensity threshold based on the average auto-fluorescence detected in the oocyte cytoplasm for both genotypes was set. The volume occupied by pixels exceeding the threshold was then determined for each oocyte.

Fluorescence recovery after photobleaching (FRAP) analysis

Individual oocytes were mounted in glass-bottom dishes as described above. A 'prebleach' *z*-series centered on the oocyte posterior cortex was taken with a 63×/1.4 NA oil immersion objective and a 4× optical zoom. A small 15-25 μm thick region of interest (ROI) at the posterior cortex was bleached to 40-60% of the initial fluorescence by bleaching successive 2 μm sections at maximum 488, 458 and 476 laser intensity for a total of 20 iterations. Recovery was monitored by collecting a *z*-series every two minutes after bleaching. After background correction, the mean intensity of the ROI for each time point was normalized to the initial fluorescence (100%).

Statistical analysis

All data were analyzed using PRISM 5.0 (Graphpad). For quantification of pole cell and live-imaging data, normal distributions were confirmed using the D'Agnostino-Pearson normality test and Student's *t*-test was used to determine significance (Zimyanin et al., 2008).

RESULTS

Purification and identification of Lost

The *nos* localization signal, located within the *nos* 3′UTR, comprises multiple localization elements with partially redundant functions (Gavis et al., 1996; Bergsten and Gavis, 1999). Previously, we performed tandem RNA affinity purification using one of these elements, the 88 nucleotide +2′ localization element, to isolate *nos* localization factors. Mass spectrometry analysis identified Rump, the *Drosophila* hnRNP M homolog, which we validated as a direct-acting *nos* localization factor (Jain and Gavis, 2008). In addition to the peptides corresponding to Rump, 50 peptides were recovered that represent much of the 545 amino acids of the predicted protein encoded by the gene CG14648 (Flybase). CG14648, which we have named *lost*, was previously identified in a screen of GFP protein-trap insertions for proteins localized to ovarian RNP-containing structures called sponge bodies and has been listed as component of several RNP complexes isolated from cultured cells, but has never been characterized (Blagden et al., 2009; Herold et al., 2009; Snee and Macdonald, 2009; Worringer et al., 2009). The predicted Lost polypeptide contains a putative 5-formyltetrahydrofolate cyclo-ligase domain that is 35% identical to human 5-FTHF cyclo-ligase domains. FTHF cyclo-ligases are essential components of folate metabolism in humans (Dayan et al., 1995; Anguera et al., 2003), but it is currently unknown if and how this domain functions in *Drosophila*. Notably, there are no conserved protein-protein or RNA-binding domains that would shed light on a role for Lost in mRNA localization.

Lost and Rump interact biochemically

Whereas Rump binds directly to the *nos* +2′ element used for purification (Jain and Gavis, 2008), we were unable to detect direct binding by recombinant Lost protein to this element or any other region of the *nos* 3′UTR (see below and data not shown). Inclusion of recombinant Rump in the binding reactions also had no effect. These results suggest that Lost associates indirectly with the *nos* localization signal, via its interaction with one or more components of the *nos* RNP.

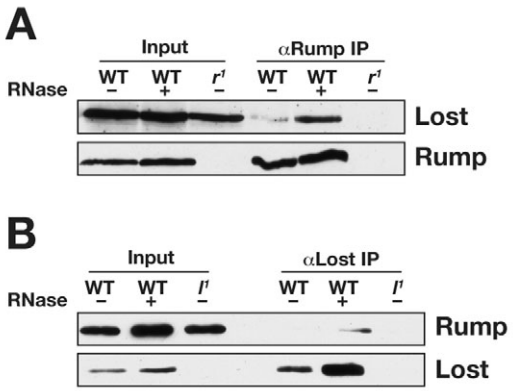

Fig. 1. Lost interacts with the *nos* localization factor Rump. (**A**,**B**) Co-immunoprecipitation analysis of Rump (A) and Lost (B) from wild-type (WT), *rump¹* (*r¹*), or *lost¹* (*l¹*) *Drosophila* ovary extracts with (+) or without (–) RNase treatment. Lost and Rump are detected by immunoblotting with the respective antibodies as indicated. The input samples contain 1-2% of the amount of extract used for immunoprecipitation (IP). The enhancement of co-immunoprecipitation in the presence of RNase could be due to protein conformational changes that result in enhanced antibody or increased protein accessibility.

Because Rump was isolated in the same purification as Lost and binds directly to the *nos* 3′UTR, we tested whether Lost interacts with Rump. Rump-containing complexes were immunopurified from ovary extract using an anti-Rump antibody and analyzed by immunoblotting with a monoclonal antibody generated against Lost protein (see Fig. S1 in the supplementary material). Lost is detected specifically in anti-Rump immunoprecipitates from wild-type ovary extract but not from *rump* mutant ovary extract, which lacks Rump protein (Fig. 1A). Similarly, Rump and Lost are co-immunoprecipitated by anti-Lost antibody from wild-type ovary extract but not from extract prepared from ovaries that lack Lost protein (see below) (Fig. 1B). The interaction of Lost and Rump is insensitive to RNase treatment of the extract under conditions shown to disrupt RNA-dependent interactions (Kalifa et al., 2009) (Fig. 1A,B). The RNA-independent interaction of Lost with Rump suggests that Lost was purified as a *nos* RNP component by association with Rump.

Lost is a cytoplasmic protein that is posteriorly enriched in the oocyte and early embryo

We took advantage of a protein-trap P element inserted in the *lost* gene ($CG14648^{ZCL3169}$; Fig. 2A) (Morin et al., 2001) to monitor the distribution of Lost. GFP-Lost flies express *lost* at near wild-type levels (Fig. 2B), produce protein recognized by an anti-Lost antibody and have no overt phenotype (data not shown), suggesting that the GFP insertion does not disrupt *lost* function. GFP-Lost is cytoplasmic in the nurse cells and in the oocyte, where it becomes enriched early in oogenesis (Fig. 2C). During mid-oogenesis, GFP-Lost appears to be concentrated at the anterior margin of the oocyte (Fig. 2C,D) and is also detected weakly at the posterior cortex (Fig. 2C,D). GFP-Lost is cortical in late stage oocytes, enriched both anteriorly and posteriorly (Fig. 2E). This cortical distribution

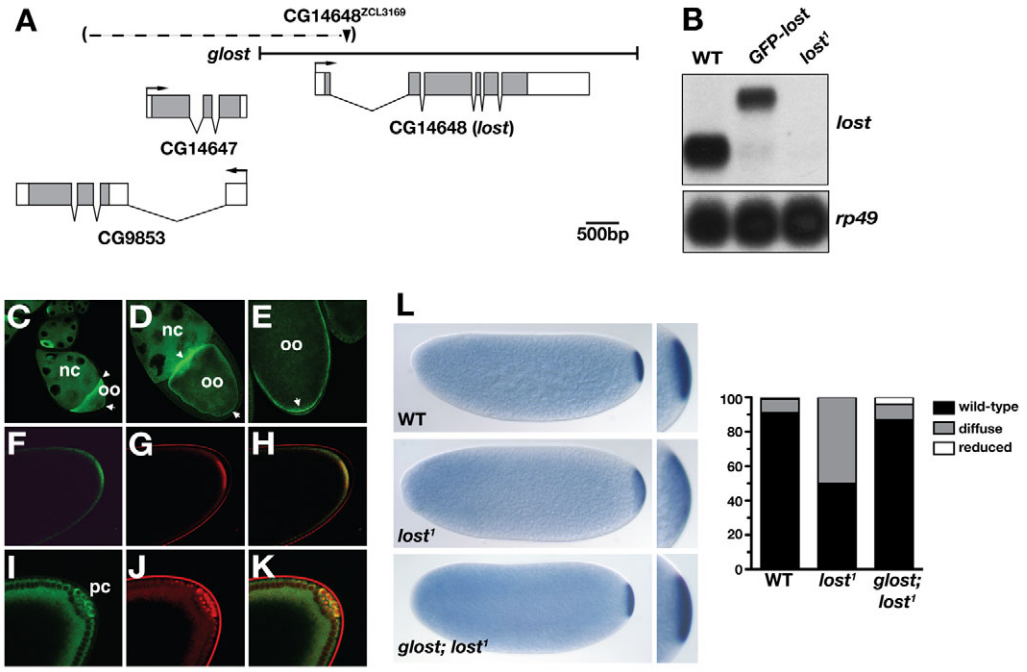

Fig. 2. Identification and characterization of Lost. (**A**) Genomic region surrounding the CG14648 (*lost*) locus, including upstream genes CG14647 and CG9853. The organization of the *lost* transcript, including the predicted transcriptional start site, is shown with coding sequence indicated in gray and 5′ and 3′ UTRs in white. FlyBase predicts an additional transcriptional start site but the coding potential of the transcript is unclear and we have no evidence of an additional isoform. The arrowhead marks the site of the GFP gene-trap *P* element insertion CG14648^{ZCL3169} in the first intron; the extent of the *lost*^{1} lesion created by imprecise excision of this P element is indicated by the dashed line and parentheses. The deletion removes both of the predicted CG14648 transcriptional start sites. The region contained in the genomic *lost* rescue transgene (*glost*) is indicated. (**B**) Northern blot analysis of *lost* mRNA in wild-type (WT), CG14648^{ZCL3169} (GFP-*lost*) and *lost*^{1} ovaries. *rp49* serves as a loading control. (**C-E**) Confocal images of GFP-Lost (green) in fixed stage 7-8 (C), stage 10 (D) and stage 13 (E) egg chambers. Arrowheads indicate anterior enrichment, arrows indicate posterior enrichment. nc, nurse cells; oo, oocyte. (**F-K**) Confocal images showing the posterior poles of live pre-blastoderm (F-H) and blastoderm stage (I-K) embryos expressing GFP-Lost (green) and *nos***RFP* (red). pc, pole cells. (**L**) In situ hybridization to *nos* mRNA in early wild-type embryos (WT), *lost*^{1} embryos or *lost*^{1} embryos with the genomic *lost* rescue transgene (*glost*; *lost*^{1}). Anterior is to the left. Right-hand panels show enlargements of the posterior for each genotype. Data from in situ hybridization were used to classify posterior localization as wild type, diffuse or reduced; quantification of these patterns is shown on the right (WT, *n*=116; *lost*^{1}, *n*=292; *glost*; *lost*^{1}, *n*=103).

persists in the early embryo, with GFP-Lost enriched only at the posterior cortex, coincident with *nos* (Fig. 2F-H). Subsequently, GFP-Lost is incorporated along with *nos* into the pole cells (Fig. 2I-K). The selective enrichment of Lost with *nos* in the early embryo and pole cells is consistent with a role as a posterior localization factor.

Isolation of a *lost* null allele

We generated a *lost* mutation, *lost*^{1}, by excision of the protein-trap P element. Imprecise excision of this P element resulted in an ~4 kb deletion that includes the predicted transcriptional start site (Fig. 2A). Northern blot analysis and immunoblotting with anti-Lost antibody show that both *lost* mRNA and Lost protein are missing from *lost*^{1} ovaries (Fig. 2B; see Fig. S1 in the supplementary material). Females homozygous for *lost*^{1} are fertile but, similar to the defect seen in *rump* mutants (Jain and Gavis, 2008), homozygous *lost*^{1} males are sterile. Also similarly to *rump* mutants, *lost*^{1} females exhibit a maternal-effect defect, with 59% of embryos produced (*n*=954) failing to develop. Of those that complete embryogenesis, 7% show mild abdominal segmentation defects (partial deletions or fusions of segments; data not shown). Although the *lost* deletion disrupts two additional genes of unknown function, CG14647 and CG9853 (Fig. 2A), all of the *lost*^{1} phenotypes described here and below can be rescued by a single copy of a genomic *lost* transgene (*glost*, Fig. 2A), indicating that these phenotypes are due to elimination of *lost* function specifically and not due to disruption of the neighboring genes.

lost mutants exhibit a mild *nos* localization defect

A role for *lost* in *nos* localization was first investigated by performing in situ hybridization to *nos* in embryos from *lost*^{1} mutant females (referred to hereafter as *lost*$^{-}$ embryos). In 50% of *lost*$^{-}$ embryos, localization of *nos* appears more diffuse than in wild-type embryos and the wild-type distribution is restored by expression of the *lost* transgene (Fig. 2L). Like the mild phenotype of *rump* mutants, the modest but rescuable *nos* localization and abdominal segmentation defects observed in *lost* mutants suggest that Lost acts redundantly with or in parallel to other *nos* localization factors. Such redundancy among *nos* localization factors is predicted by the partial functional redundancy exhibited by *nos* localization signal elements (Gavis et al., 1996; Bergsten and Gavis, 1999).

An unanticipated requirement for Lost and Rump in *osk* localization

To determine whether the biochemical interaction between Lost and Rump reflects a collaborative role in *nos* localization, we generated flies mutant for both *lost* and *rump* (*lost*$^{-}$ *rump*$^{-}$).

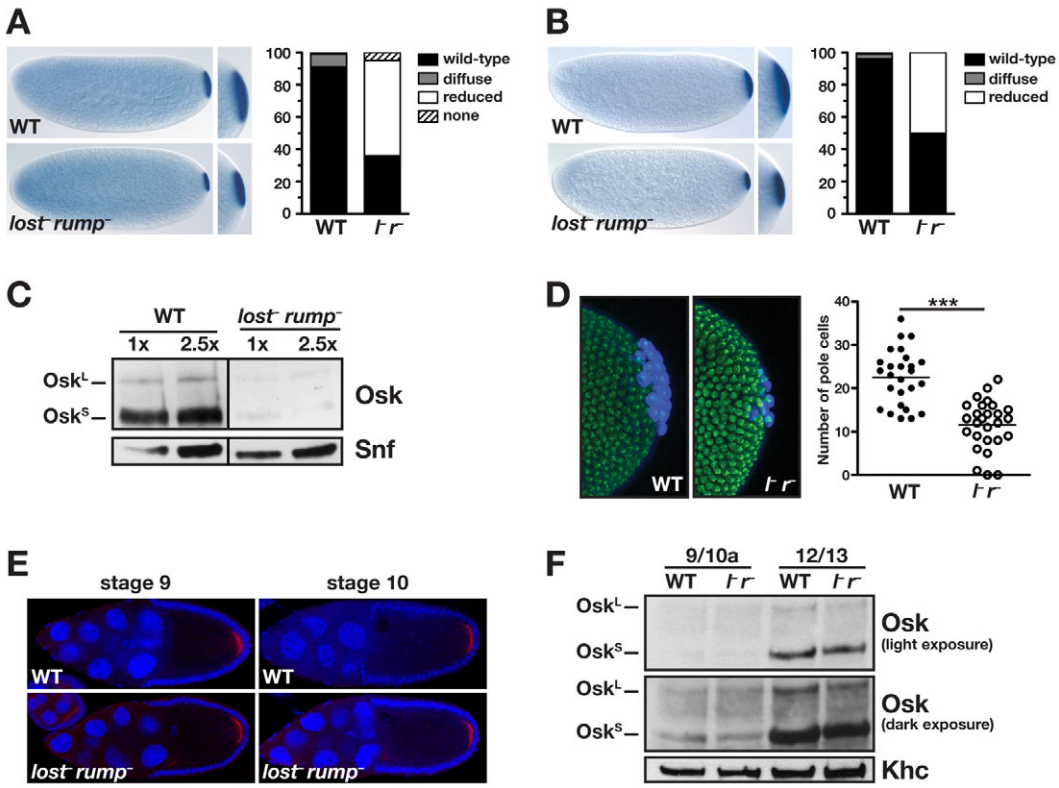

Fig. 3. Lost and Rump are required for *osk* localization. (**A**,**B**) In situ hybridization to *nos* (A) or *osk* (B) in early wild-type (WT) or *lost*⁻ *rump*⁻ embryos. Right-hand panels show enlargements of the posterior for each genotype. Quantification of posterior localization patterns observed by in situ hybridization is shown on the right for each mRNA (*nos*: WT, *n*=116; *lost*⁻ *rump*⁻, *n*=85. *osk*: WT, *n*=166; *lost*⁻ *rump*⁻, *n*=60). (**C**) Immunoblot analysis of Osk levels in wild-type (WT) or *lost*⁻ *rump*⁻ 0- to 2-hour-old embryo extracts. Both protein isoforms, Osk^L and Osk^S, can be detected in all wild-type and *lost*⁻ *rump*⁻ samples. Densitometry analysis shows that Osk is reduced by ~75% in *lost*⁻ *rump*⁻ embryos compared with wild type. Snf serves as loading control. (**D**) Confocal *z*-series projections showing the posterior of wild-type (WT) or *lost*⁻ *rump*⁻ (*l*⁻ *r*⁻) blastoderm embryos immunostained for Vas (Blue). Nuclei are labeled with DAPI (green). Graph shows the total number of pole cells per embryo (solid circles for WT, open circles for *lost*⁻ *rump*⁻), determined by counting cells that were both Vas- and DAPI-positive. The average number of pole cells in *lost*⁻ *rump*⁻ embryos is significantly less than the wild-type average ($P<0.0001$). (**E**) Fluorescence in situ hybridization to *osk* (red) in wild-type (WT) or *lost*⁻ *rump*⁻ egg chambers at the indicated stages. Nuclei are stained with DAPI (blue). Anterior is to the left. All of stage 9 *lost*⁻ *rump*⁻ oocytes (*n*=33) and 98% of stage 10 *lost*⁻ *rump*⁻ oocytes (*n*=52) exhibit normal posterior accumulation of *osk* mRNA. (**F**) Immunoblot analysis of Osk in extracts from wild-type (WT) or *lost*⁻ *rump*⁻ (*l*⁻ *r*⁻) oocytes at mid-oogenesis (stage 9/10a) and late oogenesis (stage 12/13). Kinesin heavy chain (Khc) provides a loading control. Densitometry analysis shows no difference in the total amount of Osk protein between mid-stage wild-type and *lost*⁻ *rump*⁻ oocytes (<5%, darker exposure). By contrast, total Osk is reduced by 30% in late-stage *lost*⁻ *rump*⁻ oocytes compared with wild type (lighter exposure).

Similarly to the individual mutants, *lost*⁻ *rump*⁻ females exhibit a maternal-effect defect, with 54% of their embryos (*n*=1905) failing to develop. However, abdominal segmentation defects (primarily loss of one segment or partial deletions and fusions of segments) are more prevalent among the surviving *lost*⁻ *rump*⁻ progeny (18%) than for either *lost*⁻ (7%) or *rump*⁻ (11%) embryos. Moreover, in contrast to *lost* or *rump* mutant embryos, the double mutant embryos show a dramatic decrease in posterior accumulation of *nos* without affecting overall *nos* levels (Fig. 3A, data not shown). In 64% of *lost*⁻ *rump*⁻ embryos, *nos* localization is eliminated or reduced to a small posterior disc (Fig. 3A). In addition, Nos protein levels are dramatically reduced compared with wild type (data not shown), consistent with reduced abdominal segmentation. Presumably, many of the embryos with reduced *nos* localization are among the population that fails to develop, leading to the difference in the frequencies of localization and segmentation defects.

To our surprise, we found that localization of *osk* is similarly affected in *lost*⁻ *rump*⁻ embryos. Despite wild-type *osk* levels (data not shown), *osk* localization is reduced to a small disc in 50% of *lost*⁻ *rump*⁻ embryos (Fig. 3B). Consequently, in *lost*⁻ *rump*⁻ embryos, Osk is reduced to less than 25% of the wild-type level (Fig. 3C). Consistent with previous observations that pole cell formation is highly sensitive to Osk levels, we find that *lost*⁻ *rump*⁻ embryos have significantly fewer pole cells than wild-type embryos (*lost*⁻ *rump*⁻ average=11.5, *n*=27; wild-type average=22.5, *n*=26; Fig. 3D). We have previously shown that *osk* localization is not affected in *rump* mutant embryos (Jain and Gavis, 2008). Elimination of *lost* alone has only a minor effect, with *osk* appearing less tightly localized in 13% of *lost*⁻ embryos (see Fig. S2 in the supplementary material). Like the more prevalent *nos* localization defect, this phenotype is rescued by the genomic *lost* transgene (see Fig. S2 in the supplementary material). Eliminating both *lost* and *rump* function thus has a far more dramatic mRNA

localization phenotype than mutations in either gene alone. These results reveal redundant or overlapping contributions by *lost* and *rump* in mediating *osk* as well as *nos* localization. The anteriorly localized *bcd* is unaffected in *lost⁻ rump⁻* embryos (see Fig. S3A in the supplementary material), indicating specificity of *lost* and *rump* for particular localization pathways.

lost and *rump* are not required for *osk* mRNA localization during mid-oogenesis

The localized distribution of *nos* and *osk* in the embryo is the end result of transport and anchoring events occurring earlier during oogenesis. Thus, we analyzed the distribution of *osk* mRNA and Osk protein accumulation during oogenesis. *Drosophila* oogenesis can be divided into 14 morphologically defined stages, with nurse cell dumping occurring at the end of stage 10 (King, 1970). Microtubule-dependent transport of *osk* to the posterior of the oocyte occurs primarily during stage 9 and the mRNA is subsequently maintained at the posterior by a mechanism involving Osk protein and the actin cytoskeleton (Rongo et al., 1995; Babu et al., 2004; Vanzo et al., 2007; Suyama et al., 2009). In contrast to previously characterized mutants with *osk* localization defects, posterior localization of *osk* appears wild type in 100% of stage 9 egg chambers (*n*=33) and 98% of stage 10 egg chambers (*n*=52) (Fig. 3E). Consistent with this result, Osk levels are comparable between *lost⁻ rump⁻* and wild-type stage 9/10 egg chambers (Fig. 3F). Neither microtubule organization nor the anterodorsal localization of *grk* is obviously affected in *lost⁻ rump⁻* mutant egg chambers (see Fig. S3B-E in the supplementary material). Furthermore, the cortical actin cytoskeleton, including the F-actin projections induced by Osk at the oocyte posterior, appears to be unaltered in stage 9-10 *lost⁻ rump⁻* mutant oocytes (see Fig. S3G,H in the supplementary material). Taken together, these data indicate that a posterior localization pathway is specifically disrupted in *lost⁻ rump⁻* mutants.

A second phase of *osk* localization occurs coincident with nurse cell dumping

The decrease in the amount of *osk* at the posterior of *lost⁻ rump⁻* embryos could reflect a role for Lost and Rump in maintaining *osk* at the posterior cortex during the later period of oogenesis and/or fertilization. Alternatively, accumulation of *osk* in the nurse cells through stage 10 (Kim-Ha et al., 1991) suggests that additional *osk* enters the oocyte during nurse cell dumping. *lost* and *rump* might, therefore, function to promote the posterior localization of this population of *osk* during late oogenesis. Consistent with this idea, a previous study showed that synthetic *osk* RNA injected into stage 11 oocytes is capable of localizing to the posterior (Glotzer et al., 1997), although the relevance to endogenous *osk* has never been tested. To distinguish between these possibilities, we first investigated the dynamics of *osk* mRNA during late oogenesis using the transgenic MS2 tagging system to label *osk* mRNA with GFP (designated as *osk*GFP*) in vivo. Expression of ms2-tagged *osk* rescues the *osk* mutant oogenesis defect (Lin et al., 2008).

Time-lapse imaging of *osk*GFP* in cultured wild-type egg chambers reveals a second phase of *osk* localization during and after nurse cell dumping (Fig. 4A-D). Fluorescence intensity measurements show that, on average, there is a 45% increase in *osk*GFP* at the posterior as oogenesis progresses from late stage 10 (just prior to nurse cell dumping) to late stage 12 (after nurse cell dumping) (*n*=6; Fig. 4Q,Q′). Concomitantly, Osk protein levels increase dramatically post-dumping (Fig. 3F). Similarly, a previous study using an Osk-GFP reporter protein showed that Osk levels at the posterior increase during late stages of oogenesis (Snee et al., 2007). Our results suggest that a late phase of *osk* localization is most likely responsible for the observed accumulation of Osk-GFP in late oocytes. As the *osk-(ms2)$_6$* transgene introduces an extra copy of *osk*, it is possible that the second phase of *osk* accumulation could simply reflect a delay in localization due to the presence of excess *osk*. We therefore expressed *osk*GFP* in females heterozygous for an *osk* RNA null allele, *osk^{A87}* (Jenny et al., 2006), to achieve an approximately wild-type level of *osk* mRNA (see Fig. S4A-D in the supplementary material). Fluorescence intensity quantification shows that in *osk^{A87}* heterozygotes the amount of *osk*GFP* at the posterior of cortex triples by the end of nurse cell dumping (see Fig. S4E in the supplementary material). This enhancement of *osk*GFP* localization probably reflects the alleviation of competition between transgenic *osk*GFP* mRNA and wild-type *osk* mRNA for a limiting posterior anchor.

To confirm the dynamic behavior of *osk* at the posterior, we performed fluorescence recovery after photobleaching (FRAP) experiments on early stage 12 wild-type oocytes that were still undergoing ooplasmic streaming. The fluorescence from *osk*GFP* was irreversibly inactivated in a small, three-dimensional region of interest (ROI) at the posterior cortex by high-intensity illumination, and fluorescence recovery in the ROI volume was monitored over time (Fig. 4E-H). Notably, fluorescence in the ROI increases steadily throughout the recovery time course, even surpassing the initial fluorescence levels in two of the three oocytes monitored (Fig. 4R, data not shown). These data, together with the results from our time-lapse imaging studies, provide strong evidence that *osk*GFP* continues to accumulate at the posterior cortex throughout the period of ooplasmic streaming. We cannot, however, rule out the possibility that local reorganization of RNPs anchored in adjacent regions of the cortex might, in part, contribute to the recovery of *osk*GFP*.

The second phase of *osk* accumulation fails to occur in *lost rump* mutants

Consistent with the in situ hybridization results, *osk*GFP* localization is indistinguishable between *lost⁻ rump⁻* and wild-type egg chambers at stages 9 and 10 (data not shown). By contrast, imaging of stage 12 and 13 egg chambers reveals a dramatic decrease in the amount of *osk*GFP* at the posterior of the double mutants relative to wild type (Fig. 4I-L). Moreover, time-lapse imaging of individual egg chambers shows that, on average, the amount of *osk*GFP* at the posterior cortex decreases by 77% between stages 10B and 12 (*n*=5; Fig. 4Q,Q′). This is in stark contrast to the 45% increase in posteriorly localized *osk*GFP* observed in wild-type oocytes (Fig. 4Q,Q′). Thus, not only is the second phase of *osk* localization attenuated in *lost⁻ rump⁻* oocytes, but *osk*GFP* localized during mid-oogenesis is not maintained at later stages of oogenesis despite the presence of an intact actin cytoskeleton (Fig. 4I-L,Q,Q′; see Fig. S3G-H in the supplementary material). Furthermore, quantification of Osk levels in stage 12 and 13 egg chambers shows a 30% decrease in Osk in *lost⁻ rump⁻* relative to wild type (Fig. 3F). The mRNA localization defect, resulting in diminished production of Osk throughout the remainder of oogenesis, explains the loss of localized *osk* mRNA and Osk protein observed in *lost⁻ rump⁻* embryos (Fig. 3B,C).

Despite reduced accumulation of *osk*GFP* at the posterior of stage 12 *lost⁻ rump⁻* oocytes, we were able to perform FRAP analysis. *osk*GFP* fluorescence shows substantial recovery in the three-dimensional ROI, but unlike the wild-type case, the

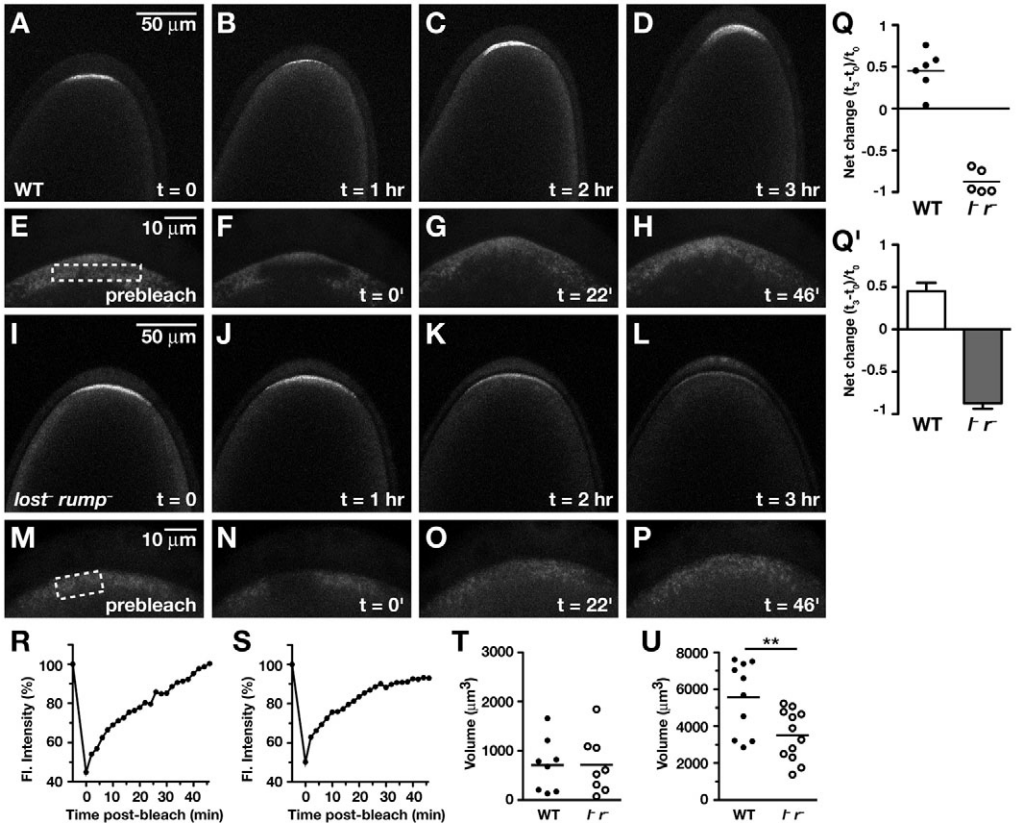

Fig. 4. Continued accumulation of germ plasm during late stages of oogenesis. (**A-D**) Time-lapse confocal projections of the posterior of a live *Drosophila* oocyte expressing *osk*GFP*. The time course captures the localization of *osk*GFP* starting prior to the onset of nurse cell dumping, stage 10B (A), and ending after nurse cell dumping is complete, stage 12 (D). Elapsed time (t) is indicated; posterior is up. (**E-H**) Fluorescence recovery after photobleaching (FRAP) experiment performed on *osk*GFP* at the posterior of a wild-type stage 12 oocyte. The photobleached region of interest (ROI) is indicated by the rectangle. The zero time point corresponds to the completion of photobleaching in the ROI. Time elapsed in the FRAP recovery period is indicated; posterior is up. (**I-L**) Time-lapse confocal projections of *osk*GFP* at the posterior of a live *lost⁻ rump⁻* oocyte from stage 10B (I) to stage 12 (L). Elapsed time is indicated; posterior is up. (**M-P**) FRAP experiment performed on *osk*GFP* at the posterior of a stage 12 *lost⁻ rump⁻* oocyte. The photobleached ROI is indicated by the rectangle. The zero time point corresponds to the completion of photobleaching in the ROI. Time elapsed in the FRAP recovery period is indicated; posterior is up. (**Q**,**Q′**) The total amount of posterior *osk*GFP* fluorescence in time-lapse confocal *z*-stack images was quantified for six wild-type and five *lost⁻ rump⁻* oocytes (see Materials and methods) and the net change in fluorescence intensity between the initial time point (equivalent to panels A or I, labeled as t_0) and final time point (equivalent to panels D or L, labeled as t_3) was plotted for each oocyte (Q). Plot of the average net change in fluorescence intensity ± s.e.m. for each genotype is shown in Q′. (**R**,**S**) Quantification of the FRAP experiments from the wild-type (R) or *lost⁻ rump⁻* (S) oocytes shown in E-H and M-P. Similar results were observed for two additional wild-type and three additional *lost⁻ rump⁻* stage 12 egg chambers. (**T**,**U**) Quantification of the volume (μm^3) occupied by *osk*GFP* at the posterior of individual wild-type (solid circles) and *lost⁻ rump⁻* (open circles) oocytes at stage 10A (T) and stage 12/13 (U). The mean value for the volume of *osk*GFP* fluorescence (horizontal bars) in *lost⁻ rump⁻* oocytes is not significantly different from wild type at stage 10A but is significantly smaller by stage 12/13 ($P<0.0086$).

initial fluorescence levels are low and are not exceeded (Fig. 4M-P,S). This recovery, together with the net loss of *osk*GFP* from the posterior cortex between stages 10B and 12, could be explained by dissociation of the majority of *osk* that was localized during mid-oogenesis from the cortex with a small amount of new accumulation during dumping. Alternatively, partial repopulation of the bleached region could result from local reorganization of the remaining germ plasm at the posterior cortex in the absence of new *osk* accumulation. Although we cannot yet distinguish whether one or both of these possibilities applies, results from both the time-lapse imaging and FRAP analyses demonstrate a requirement for *lost* and *rump* in the late phase accumulation and maintenance of *osk* at the posterior cortex.

In *lost⁻ rump⁻* embryos, not only is the amount of localized *osk* and *nos* reduced, but both RNAs occupy a much smaller region of the posterior cortex than they do in wild-type embryos (Fig. 3A,B). We calculated the total volume occupied by *osk*GFP* at the posterior of wild-type and *lost⁻ rump⁻* oocytes in staged egg chambers using identical conditions for imaging and quantification for all samples (see Materials and methods). At stage 10A, *osk*GFP* occupies the same mean volume in wild-type or *lost⁻ rump⁻* oocytes (Fig. 4T). However, by late stage 12/early stage 13, the mean volume of *osk*GFP* at the posterior in *lost⁻ rump⁻* oocytes is 63% of its mean volume in wild-type oocytes (Fig. 4U). Taken together, these data suggest that the failure to accumulate additional *osk* mRNA during late stages of oogenesis results in failure of the germ plasm to expand in volume proportionate to the

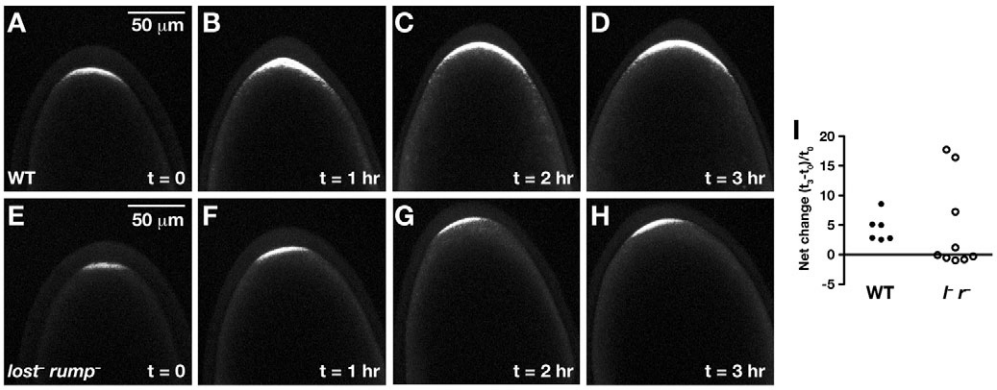

Fig. 5. **Continued posterior accumulation of GFP-Vasa during late oogenesis is dependent on *lost* and *rump*.** (**A-H**) Time-lapse confocal projections of the posterior of live wild-type (A-D) and *lost*⁻ *rump*⁻ (E-H) oocytes expressing GFP-Vas, from stage 10B (A,E) to stage 12 (D,H). Elapsed time (t) is indicated; posterior is up. (**I**) The net change in the total amount of GFP-Vas fluorescence at the posterior of individual wild-type (WT, solid circles; *n*=6) and *lost*⁻ *rump*⁻ (open circles; *n*=9) oocytes between t_0 and t_3 was quantified as described in Fig. 4.

size of the growing oocyte and, consequently, only a small disc of localized germ plasm is observed in the embryo. Examination of *nos***GFP* in stage 14 oocytes showed that *nos* localization is affected in parallel to *osk*, leading to the reduction of localized *nos* mRNA and Nos protein in the embryo (see Fig. S5 in the supplementary material, data not shown).

A late phase of Vas accumulation

To determine whether protein components of the germ plasm also continue to accumulate late in oogenesis, we performed similar time-lapse imaging of GFP-Vas, localization of which during mid-oogenesis depends on Osk. After the onset of nurse cell dumping, posteriorly localized GFP-Vas becomes visibly enhanced in wild-type oocytes and by stage 12, there is on average five times more GFP-Vas at the posterior compared with stage 10B (*n*=6; Fig. 5A-D,I). By contrast, Vas does not accumulate to wild-type levels in the majority of *lost*⁻ *rump*⁻ mutant egg chambers during this time (*n*=9; Fig. 5E-I). Moreover, five of the nine *lost*⁻ *rump*⁻ oocytes assayed exhibit loss of GFP-Vas at the posterior from stage 10B to 12 (Fig. 5I). Thus, the continued accumulation of *osk* mRNA and Osk protein leads to an amplification of the germ plasm at late stages of oogenesis.

Lost and Rump associate with *nos* and *osk* RNPs in vivo

We hypothesized that Rump and Lost might interact directly with *osk* mRNA to mediate the late phase of *osk* localization. Thus, we performed UV-crosslinking of purified recombinant MBP-Rump or MBP-Lost to radiolabeled *osk* 5′UTR and 3′UTR RNA probes. The *nos* +2′ element RNA probe previously shown to bind to Rump (Jain and Gavis, 2008) was included for comparison. Whereas Rump interacts with the *nos* +2′ element and the *osk* 3′UTR, no binding is detected to the *osk* 5′UTR (Fig. 6A). In contrast to MBP-Rump, MBP-Lost does not bind to any of the RNAs tested (Fig. 6A). Similar results have been obtained from independent preparations of MBP-Lost protein.

Rump binds specifically to two CGUU motifs within the *nos* +2′ element (Jain and Gavis, 2008). The *osk* 3′UTR also contains two CGUU motifs, suggesting that they might be responsible for the interaction with Rump. We therefore divided the *osk* 3′UTR into a 5′ fragment (nucleotides 1-738) without the putative Rump binding sites and a 3′ fragment (nucleotides 731-1004) containing these sites and performed UV-crosslinking with MBP-Rump. Unexpectedly, MBP-Rump binds to both fragments (Fig. 6B), indicating that Rump recognizes at least one novel binding site in the *osk* 3′UTR.

We have previously shown that Rump forms a complex with *nos* mRNA in vivo. To determine whether Rump interacts with *osk* mRNA in vivo, we immunoprecipitated Rump from wild-type or *rump* mutant ovary extract and analyzed co-purifying RNA by RT-PCR. *osk* is detected in the immunoprecipitate from wild-type extract, but not from *rump*⁻ extract (Fig. 6C). In addition, Rump forms a complex with *osk* in the *lost*⁻ extract (data not shown), indicating that the interaction of Rump with *osk* in vivo, like the interaction in vitro, does not depend on Lost. Taken together with previous observations (Jain and Gavis, 2008), these results suggest that Rump recognizes mRNAs designated for posterior localization and recruits Lost to these RNP complexes to mediate localization at late stages of oogenesis.

DISCUSSION

Posterior localization of *osk* underlies the formation of germ plasm at the posterior of the oocyte and, ultimately, the development of the germ line and abdomen of the animal. Whereas *osk* localization during mid-oogenesis has been well studied, we have now identified a second, previously uncharacterized phase of *osk* localization that occurs late in oogenesis, beginning with nurse cell dumping. The concomitant accumulation of Vas at the posterior during this period indicates that this phase of *osk* localization leads to germ plasm amplification. This late phase of *osk* localization specifically requires Rump, which binds to *osk*, and Lost, which interacts with Rump. In *lost*⁻ *rump*⁻ embryos, the reduction of germ plasm at the posterior leads to fewer germ cells and abdominal segmentation defects. Thus, the localization of *osk* during mid-oogenesis is not sufficient to ensure wild-type germline and abdominal development. Rather, the second phase of *osk* localization and germ plasm accumulation is crucial for embryogenesis. Our results are consistent with results from a previous study showing that continued production of Osk during late stages of oogenesis is essential for abdomen formation (Snee et al., 2007) and they reveal the mechanism behind this accumulation.

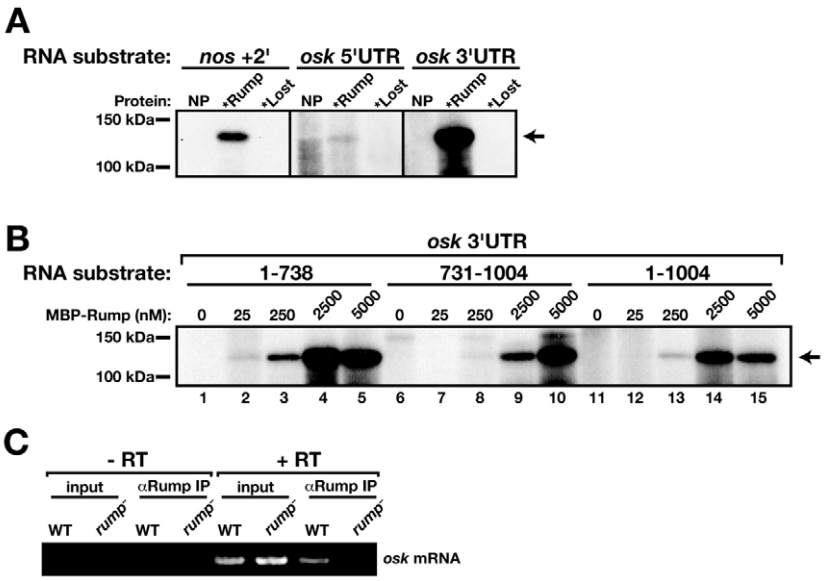

Fig. 6. Rump associates with *osk* both in vitro and in vivo. (**A**) UV-crosslinking of MBP-Rump (*Rump) or MBP-Lost (*Lost) to ^{32}P-labeled *nos* +2′, *osk* 5′UTR, or *osk* 3′UTR RNA probes. The protein-RNA complex is indicated by the arrow. NP, no protein added. (**B**) UV-crosslinking of MBP-Rump to ^{32}P-labeled probes comprising *osk* 3′UTR nucleotides 1-738, nucleotides 731-1004, or the entire *osk* 3′UTR (nucleotides 1-1004). Binding reactions contained increasing concentrations of MBP-Rump as indicated. The Rump-*osk* complex is indicated by the arrow. (**C**) RT-PCR to detect *osk* co-immunoprecipitated with Rump from wild-type (WT) and *rump*$^{-}$ ovary extracts. Reactions were performed without (–RT) or with (+RT) reverse transcriptase. *rump*$^{-}$ extract serves as a negative control to demonstrate antibody specificity.

The failure of *osk* to accumulate at the posterior of *lost*$^{-}$ *rump*$^{-}$ mutants at late stages of oogenesis could result from the failure of *osk* to reach to the oocyte posterior altogether or the failure to become entrapped and anchored there. Nurse cell dumping and ooplasmic streaming occur normally in *lost*$^{-}$ *rump*$^{-}$ mutants (see Fig. S3E,F in the supplementary material), suggesting that the defect does not lie in the ability of *osk* to reach the posterior cortex. The lack of localized *osk* in embryos from mutants such as *staufen*, which disrupt *osk* localization during mid-oogenesis, or *osk* mis-sense mutants, which lack functional Osk protein and fail to maintain *osk* at the posterior after stage 9, suggests that the late phase of *osk* localization depends on the prior localization and translation of Osk and recruitment of germ plasm components during mid-oogenesis (Ephrussi et al., 1991; Kim-Ha et al., 1991; St Johnston et al., 1991). Consistent with this evidence, Osk is required for posterior accumulation of synthetic *osk* mRNA following injection into stage 11 oocytes (Glotzer et al., 1997). Thus, Rump and Lost probably mediate the interaction of *osk* with pre-existing Osk or other germ plasm proteins, and/or the actin cytoskeleton. Eliminating both Rump and Lost produces a more severe RNA localization defect than eliminating either one but does not completely abolish localization. Partially redundant contributions by RNA-binding factors like Rump has been previously predicted for the *osk* and *nos* RNA localization signals (Kim-Ha et al., 1993; Bergsten and Gavis, 1999). Our results suggest that there is functional overlap among higher order interactions of RNA-binding proteins and adaptors like Lost that make that RNP assembly and function robust to perturbation.

Not only is the late phase of *osk* localization affected in *lost*$^{-}$ *rump*$^{-}$ mutants, but *osk* that had accumulated at the posterior of the oocyte during mid-oogenesis is de-localized. Although difficult to quantify, we also notice a transient decrease in *osk* at the posterior in wild-type oocytes immediately following the onset of nurse cell dumping (see Fig. 4A-C). One possible explanation is that the Osk-dependent anchoring mechanism established during mid-oogenesis cannot withstand the force of ooplasmic streaming and is, therefore, unable to maintain *osk* at the posterior cortex. Retention of both previously anchored and newly arriving *osk* at the cortex would, therefore, require the transition to a more robust anchoring system, through the activity of Rump and Lost. Once established, this anchor would support the continued accumulation of germ plasm through the remainder of oogenesis.

Because *nos* localization depends on the germ plasm, the *nos* localization defect observed in *lost*$^{-}$ *rump*$^{-}$ oocytes and embryos could be secondary to the *osk* localization defect. However, several pieces of evidence suggest that *lost* and *rump* might also regulate *nos* localization in parallel. Rump and Lost were both isolated by co-purification with the *nos* +2′ localization element. Rump binds to a specific sequence motif in the *nos* +2′ localization element, and mutation of these sequences or elimination of Rump compromises +2′ element localization function independently of *osk* localization. Finally, *nos* localization is frequently more diffuse in *lost* mutants whereas *osk* is largely unaffected. As an attractive hypothesis, *nos* might be transported to or anchored at the posterior together with *osk*, as part of the same RNP. Incorporation of *nos* and *osk* into this RNP and/or the ability to interact with Osk or other anchoring factors would then depend on the interaction of Lost and Rump with each mRNA. Alternatively, Lost and Rump might contribute to the assembly of an independent *nos* RNP that is competent to associate with the germ plasm at the posterior pole. Development of methods to image *osk* and *nos* simultaneously during late oogenesis will be crucial to distinguish between these possibilities.

We have previously shown that a late-acting localization pathway is responsible for the majority of anteriorly localized *bcd* in the embryo (Weil et al., 2006). The late phase of *bcd* localization is genetically distinct from *bcd* localization during mid-oogenesis but does not depend on Rump or Lost, indicating that these proteins are specific for posterior localization at late stages. Taken together, our results indicate that mRNA localization pathways functioning during late stages of oogenesis amplify localized mRNA distributions generated during mid-oogenesis to endow the embryo with the requisite concentrations of determinant mRNAs and germ plasm components needed for body axis and germline development. Our work suggests that localization factors such as Lost and Rump adapt mRNAs for utilization of multiple, mechanistically distinct localization pathways necessitated by dramatic changes in ovarian physiology and the oocyte cytoskeleton during oogenesis.

Acknowledgements
We thank T. Chou and W. Chia for fly stocks; P. Schedl, P. Lasko and A. Ephrussi for antibodies; J. Goodhouse for assistance with confocal microscopy; and E. Olesnicky Killian and J. Lee for comments on the manuscript. This work was supported by an NSF Predoctoral Fellowship (R.A.J.), an NCI training grant (K.S.S., T32CA09528) and grants from the National Institutes of Health to E.R.G. (R01GM067758) and K.S.S. (F32GM087005). Deposited in PMC for release after 12 months.

Competing interests statement
The authors declare no competing financial interests.

Supplementary material
Supplementary material for this article is available at
http://dev.biologists.org/lookup/suppl/doi:10.1242/dev.065029/-/DC1

References
Anguera, M. C., Suh, J. R., Ghandour, H., Nasrallah, I. M., Selhub, J. and Stover, P. J. (2003). Methenyltetrahydrofolate synthetase regulates folate turnover and accumulation. *J. Biol. Chem.* **278**, 29856-29862.
Babu, K., Cai, Y., Bahri, S., Yang, X. and Chia, W. (2004). Roles of Bifocal, Homer, and F-actin in anchoring Oskar to the posterior cortex of *Drosophila* oocytes. *Genes Dev.* **18**, 138-143.
Becalska, A. N. and Gavis, E. R. (2010). Bazooka regulates microtubule organization and spatial restriction of germ plasm assembly in the Drosophila oocyte. *Dev. Biol.* **340**, 528-538.
Becalska, A. N., Kim, Y. R., Belletier, N. G., Lerit, D. A., Sinsimer, K. S. and Gavis, E. R. (2011). Aubergine is a component of a *nanos* mRNA localization complex. *Dev. Biol.* **349**, 46-52.
Bergsten, S. E. and Gavis, E. R. (1999). Role for mRNA localization in translational activation but not spatial restriction of *nanos* RNA. *Development* **126**, 659-669.
Bergsten, S. E., Huang, T., Chatterjee, S. and Gavis, E. R. (2001). Recognition and long-range interactions of a minimal *nanos* RNA localization signal element. *Development* **128**, 427-435.
Blagden, S. P., Gatt, M. K., Archambault, V., Lada, K., Ichihara, K., Lilley, K. S., Inoue, Y. H. and Glover, D. M. (2009). *Drosophila* Larp associates with poly(A)-binding protein and is required for male fertility and syncytial embryo development. *Dev. Biol.* **334**, 186-197.
Brechbiel, J. L. and Gavis, E. R. (2008). Spatial regulation of *nanos* is required for its function in dendrite morphogenesis. *Curr. Biol.* **18**, 745-750.
Breitwieser, W., Markussen, F. H., Horstmann, H. and Ephrussi, A. (1996). Oskar protein interaction with Vasa represents an essential step in polar granule assembly. *Genes Dev.* **10**, 2179-2188.
Brendza, R. P., Serbus, L. R., Duffy, J. B. and Saxton, W. M. (2000). A function for kinesin I in the posterior transport of *oskar* mRNA and Staufen protein. *Science* **289**, 2120-2122.
Dayan, A., Bertrand, R., Beauchemin, M., Chahla, D., Mamo, A., Filion, M., Skup, D., Massie, B. and Jolivet, J. (1995). Cloning and characterization of the human 5,10-methenyltetrahydrofolate synthetase-encoding cDNA. *Gene* **165**, 307-311.
Ephrussi, A., Dickinson, L. K. and Lehmann, R. (1991). Oskar organizes the germ plasm and directs localization of the posterior determinant *nanos*. *Cell* **66**, 37-50.
Forrest, K. M. and Gavis, E. R. (2003). Live imaging of endogenous RNA reveals a diffusion and entrapment mechanism for *nanos* mRNA localization in *Drosophila*. *Curr. Biol.* **13**, 1159-1168.
Gavis, E. R. and Lehmann, R. (1992). Localization of *nanos* RNA controls embryonic polarity. *Cell* **71**, 301-313.
Gavis, E. R. and Lehmann, R. (1994). Translational regulation of *nanos* by RNA localization. *Nature* **369**, 315-318.
Gavis, E. R., Curtis, D. and Lehmann, R. (1996). Identification of *cis*-acting sequences that control *nanos* RNA localization. *Dev. Biol.* **176**, 36-50.
Gavis, E. R., Singer, R. H. and Hüttelmaier, S. (2007). Localized translation through messenger RNA localization. In *Translational Control in Biology and Medicine* (ed. J. W. B. Hershey, M. B. Mathews and N. Sonenberg), pp. 687-717. Cold Spring Harbor, NY: Cold Spring Harbor Laboratory Press.
Glotzer, J. B., Saffrich, R., Glotzer, M. and Ephrussi, A. (1997). Cytoplasmic flows localize injected *oskar* RNA in *Drosophila* oocytes. *Curr. Biol.* **7**, 326-337.
Herold, N., Will, C. L., Wolf, E., Kastner, B., Urlaub, H. and Luhrmann, R. (2009). Conservation of the protein composition and electron microscopy structure of *Drosophila melanogaster* and human spliceosomal complexes. *Mol. Cell. Biol.* **29**, 281-301.
Jain, R. A. and Gavis, E. R. (2008). The *Drosophila* hnRNP M homolog Rumpelstiltskin regulates *nanos* mRNA localization. *Development* **135**, 973-982.
Jenny, A., Hachet, O., Zavorszky, P., Cyrklaff, A., Weston, M. D., Johnston, D. S., Erdelyi, M. and Ephrussi, A. (2006). A translation-independent role of *oskar* RNA in early *Drosophila* oogenesis. *Development* **133**, 2827-2833.
Johnstone, O. and Lasko, P. (2004). Interaction with eIF5B is essential for Vasa function during development. *Development* **131**, 4167-4178.
Kalifa, Y., Huang, T., Rosen, L. N., Chatterjee, S. and Gavis, E. R. (2006). Glorund, a Drosophila hnRNP F/H homolog, is an ovarian repressor of *nanos* translation. *Dev. Cell* **10**, 291-301.
Kalifa, Y., Armenti, S. T. and Gavis, E. R. (2009). Glorund interactions in the regulation of *gurken* and *oskar* mRNAs. *Dev. Biol.* **326**, 68-74.
Kim-Ha, J., Smith, J. L. and Macdonald, P. M. (1991). *oskar* mRNA is localized to the posterior pole of the *Drosophila* oocyte. *Cell* **66**, 23-35.
Kim-Ha, J., Webster, P. J., Smith, J. L. and Macdonald, P. M. (1993). Multiple RNA regulatory elements mediate distinct steps in localization of *oskar* mRNA. *Development* **119**, 169-178.
King, R. C. (1970). *Ovarian Development in Drosophila melanogaster*. New York: Academic Press.
Kugler, J. M. and Lasko, P. (2009). Localization, anchoring and translational control of *oskar*, *gurken*, *bicoid* and *nanos* mRNA during *Drosophila* oogenesis. *Fly* **3**, 15-28.
Lewis, R. A. and Mowry, K. L. (2007). Ribonucleoprotein remodeling during RNA localization. *Differentiation* **75**, 507-518.
Lin, M. D., Jiao, X., Grima, D., Newbury, S. F., Kiledjian, M. and Chou, T. B. (2008). *Drosophila* processing bodies in oogenesis. *Dev. Biol.* **322**, 276-288.
Lindsley, D. L. and Zimm, G. G. (1992). *The Genome of Drosophila melanogaster*. San Diego, CA: Academic Press.
Markussen, F. H., Michon, A. M., Breitwieser, W. and Ephrussi, A. (1995). Translational control of *oskar* generates short OSK, the isoform that induces pole plasma assembly. *Development* **121**, 3723-3732.
Morin, X., Daneman, R., Zavortink, M. and Chia, W. (2001). A protein trap strategy to detect GFP-tagged proteins expressed from their endogenous loci in *Drosophila*. *Proc. Natl. Acad. Sci. USA* **98**, 15050-15055.
Pirotta, V. (1988). Vectors for P-mediated transformation in *Drosophila*. In *Vectors: A Survey of Molecular Cloning Vectors and their Uses* (ed. R. L. Rodriguez and D. T. Denhardt), pp. 437-456. Boston: Butterworths.
Rongo, C., Gavis, E. R. and Lehmann, R. (1995). Localization of *oskar* RNA regulates *oskar* translation and requires Oskar protein. *Development* **121**, 2737-2746.
Rubin, G. M., Hong, L., Brokstein, P., Evans-Holm, M., Frise, E., Stapleton, M. and Harvey, D. A. (2000). A *Drosophila* complementary DNA resource. *Science* **287**, 2222-2224.
Snee, M. J. and Macdonald, P. M. (2009). Dynamic organization and plasticity of sponge bodies. *Dev. Dyn.* **238**, 918-930.
Snee, M. J., Harrison, D., Yan, N. and Macdonald, P. M. (2007). A late phase of Oskar accumulation is crucial for posterior patterning of the *Drosophila* embryo, and is blocked by ectopic expression of Bruno. *Differentiation* **75**, 246-255.
St Johnston, D., Beuchle, D. and Nusslein-Volhard, C. (1991). Staufen, a gene required to localize maternal RNAs in the *Drosophila* egg. *Cell* **66**, 51-63.
Suyama, R., Jenny, A., Curado, S., Pellis-van Berkel, W. and Ephrussi, A. (2009). The actin-binding protein Lasp promotes Oskar accumulation at the posterior pole of the *Drosophila* embryo. *Development* **136**, 95-105.
Theurkauf, W. E., Smiley, S., Wong, M. L. and Alberts, B. M. (1992). Reorganization of the cytoskeleton during *Drosophila* oogenesis: implications for axis specification and intercellular transport. *Development* **115**, 923-936.
Vanzo, N., Oprins, A., Xanthakis, D., Ephrussi, A. and Rabouille, C. (2007). Stimulation of endocytosis and actin dynamics by Oskar polarizes the *Drosophila* oocyte. *Dev. Cell* **12**, 543-555.
Vanzo, N. F. and Ephrussi, A. (2002). Oskar anchoring restricts pole plasm formation to the posterior of the *Drosophila* oocyte. *Development* **129**, 3705-3714.
Wang, C., Dickinson, L. K. and Lehmann, R. (1994). Genetics of *nanos* localization in Drosophila. *Dev. Dyn.* **199**, 103-115.
Weil, T. T., Forrest, K. M. and Gavis, E. R. (2006). Localization of *bicoid* mRNA in late oocytes is maintained by continual active transport. *Dev. Cell* **11**, 251-262.
Worringer, K. A., Chu, F. and Panning, B. (2009). The zinc finger protein Zn72D and DEAD box helicase Belle interact and control *maleless* mRNA and protein levels. *BMC Mol. Biol.* **10**, 33.
Zimyanin, V. L., Belaya, K., Pecreaux, J., Gilchrist, M. J., Clark, A., Davis, I. and St Johnston, D. (2008). In vivo imaging of *oskar* mRNA transport reveals the mechanism of posterior localization. *Cell* **134**, 843-853.